POLITECNICO DI TORINO

Master's Degree Course in Mechanical Engineering

Master's Degree Thesis

Lowering the supply temperature of a District Heating Network through optimal sizing and positioning of Thermal Energy Storages

Supervisors
Prof. Vittorio VERDA
Prof. Elisa GUELPA
Eng. Martina CAPONE

Candidato
Antonio FORTE

April **13th 2021**

POLITECNICO DI TORINO

Master's Degree in Mechanical Engineering

Master's Degree Thesis

Lowering the supply temperature of a District Heating Network through optimal sizing and positioning of Thermal Energy Storages

Supervisors
Prof. Vittorio VERDA
Prof. Elisa GUELPA
Eng. Martina CAPONE

Candidate
Antonio FORTE

April 13th 2021

A Mamma, Papà e Alessia,
alle mie Tre Colonne Portanti.

Abstract

One amongst the numerous challenges in the field of District Heating (DH) consists of lowering the supply temperature of the water pumped from the central plant into the network.
A proper rise in the mass-flow rate injected from the plant should be taken into consideration though, to compensate for the aforementioned temperature reduction, as stated by the First Law of Thermodynamics.
The introduction of Thermal Energy Storages (TES) in specific points of the network – to be filled with hot water during night hours, i.e. when there is little or even no thermal request — would serve the purpose of partially relieving the increased pumping load when the heating systems are switched on, especially in correspondence of the morning peak of demand. Furthermore, it would prevent the risk associated with too high mass-flow rates that may circulate in the network – if only the central plant were in charge of supplying hot water to the end-users – and that might not be compatible with the cross sections of the pipes through which they flow.

This work aims at finding the optimal position of one storage with known capacity in an existing DHN, in such a way that it would be possible to inject hot water into the pipelines at a temperature lower than design conditions, still managing to deliver the required amount of heat to the end-users.
Several tests have been carried out, in order to investigate the factors that may affect the effectiveness of the reservoir, i.e. its capability of smoothing as much as possible the aforementioned peak of the thermal load.

Acknowledgements

When Professor Vittorio Verda and Professor Elisa Guelpa first presented me this work, the idea of being engaged in such a stimulating and challenging project immediately got me thrilled to bits.

Throughout the course of these six months I have been experiencing a whirlwind of emotions like I have never had before, being swung from self-acknowledgement to harsh disappointment, the last of which ominously threatened my self-commitment and determination.
I would have been on the verge of giving up right a few steps from the finish line, if it had not been for the caring love and constant encouragement of people who have been backing me up until this very last moment, to whom I would like to dedicate my most sincere and genuine words.

A first thanks and a further mention go to Professor Verda and Professor Guelpa – who taught me the importance of keeping the flame of my determination alive after having failed, and pushed me towards completing the last lap of this race.
Thanks to Martina Capone, whose help and advice have always been enlightening the path towards the achievement of my targets.

I definitely would not have made it so far, if it were not for my Mum Grazia, my Dad Enzo and my Sister Alessia. Whatever words would not be enough, to express how fortunate and grateful I am, to have the three of you by my side.
Dear Ale, thank you for choosing to put your books on that desk every morning, for all your sweet hugs, for all your deepest love.

Thank you for having made every single day lighter and brighter.

Thanks to my Grandma Filomena, my Grandpa Pasquale, to Luigi and Fede, to my aunt Marilena, and to my uncle Salvatore, for your everlasting and never ending love.

Thanks to Busca, who kept believing in me and pushed me to go the extra mile.

Thanks to Gabri for his precious company and support, which made our study sessions lighter, during these days of pandemic.

Thanks to Lorenzo and Mangi, who have been my travel mates and truest friends since the beginning of my adventure, here at Politecnico.

Thanks to Vale, with whom I have been sharing the most delightful and intimate moments, during the course of these five years.

Thanks to Miriam, Marco and Franz, with whom I stepped into the MSc path, and who are now among my dearest colleagues and friends.

Thanks to Federica, Alessandro, Luca, Federico, Lorenzo, Daniele and Mario. It was my deepest pleasure to spend my last year of University with you.

Thanks to Ilaria, whose love and support have been filling the distance between us since that summer evening in 2015.

Thanks to Giulia, for her delightfully contagious joy.

Thanks to my silent friends Bolle, Lore and Simo.

Thanks to Ludo, for all the love she gave me.

Thanks to Tina, Clelia, Caterina, Bersa, Borzi, Cere, Gio, Leo, Pedi, Simo, Simo and Zanzo, for all the laughs you make me do.

Thanks to the guys of the HR Team of *PoliENERGY*, for having sprayed colourful and bright shades in these grey, pandemic-affected months.

A special thanks to my pirates, Chiara and Simo, for the already unbreakable bonds we have built.

I wish you guys all the best.

Antonio

Table of Contents

List of Tables

List of Figures

Acronyms

DH
District Heating

DHN
District Heating Network

TES
Thermal Energy Storage

HOB
Heat Only Boiler

SST
Substation

DHW
Domestic Hot Water

CHPP
Combined Heat and Power Production

CHP
Combined Heat and Power

FLT
First Law of Thermodynamics

NB
Number of Branches

NN

Number of Nodes

RES

Renewable Energy Sources

Chapter 1

Introduction

The cornerstone of the technology known as DH (District Heating) is replacing local heat generation, which is typically carried out installing devices such as HOB (Heat Only Boiler)s, with a few, centralized, heat production facilities, both for domestic and industrial purposes [1].
Starting from the end of the 19th Century, when the first DHN (District Heating Network) was built in New York [2], District Heating has been standing out as a valid and always more sustainable alternative to conventional systems [3].

The energy distribution system works in the following way: hot water is produced at the central plant level, and subsequently pumped into a network of underground steel pipes, through which it flows for several kilometers, until it reaches a so-called SST (Substation), which may be regarded as the interface between the pipeline and the end-users, i.e. the buildings attached to the network, and with specific power requirements for space heating, DHW (Domestic Hot Water) production, or both of them.

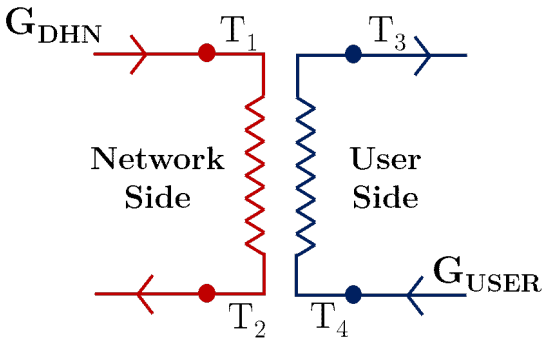

Figure 1.1: Schematic of the heat exchanger of a SST.

Every substation is equipped with a heat exchanger – schematized in Fig. 1.1 – in which the hot stream delivers thermal power to a cooler one, i.e. the water flowing through the heating terminals of the aforementioned buildings [4].
Once it has delivered heat to the user side, the cooled stream on the network (or primary) side flows through a return circuit, which has a mirrored topology with respect to the supply one, and comes back to the central plant.

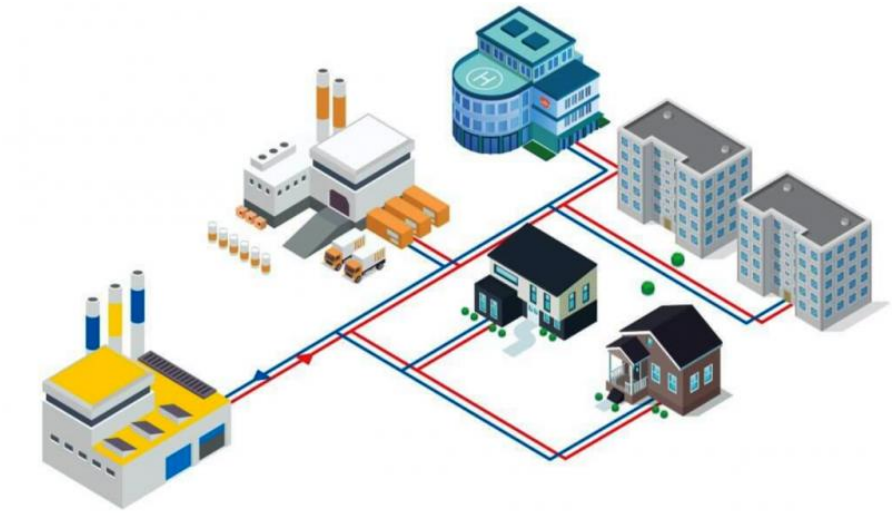

Figure 1.2: Symbolic representation of a DHN[1].

The exploitation of centralized heat production enables the consumption of a considerably lower amount of fossil fuels, with respect to the more traditional solutions. Particularly, CHPP (Combined Heat and Power Production) plays a key role in this scenario, as it perfectly matches with the way DH works.
Experimental data extracted from the DHN of Turin – a portion of which has been analyzed in this study – solidly backs up the previous statement. In fact, hot water production and supply in the city mostly rely on cogeneration from combined cycles, and numbers reveal that it takes $0.52\,MJ$ of primary energy to deliver $1\,MJ$ of energy via District Heating, in stark contrast with the figure related to, for instance, condensing boilers, which is almost doubled and equal to $0.95\,MJ$ [5].
Although being already one among the smartest technologies in the field of energy distribution, DH is continuously facing stimulating challenges towards innovation and sustainability, aiming at the development of the so-called 4th Generation District Heating (4GDH) [3]. Lowering the supply temperature of already existing networks is one of them, and is the topic addressed in this work.

[1]Source: openpr.com, available in 2021-03-30.

The main reason why such target should be pursued is that the higher the supply temperature is, the larger the thermal losses occurring between the underground pipes and the external environment would be, hence a reduced temperature would enhance the efficiency of the whole network.
Additionally, in the long-term perspective of future DH networks, a significant reduction of the supply temperature would enable to merge alternative and sustainable sources of energy with the thermal grid, such as Renewable Energy Sources (RES) [6] or waste heat from large data centres and industrial processes [7, 8].

It should be pointed out though, that lowering the aforementioned temperature has the side effect of increasing the mass-flow rate demand from every end-user, in order to guarantee that the correct amount of thermal power is delivered to the secondary side of the SST or, in other words, that it is possible to maintain the desired room temperature inside the buildings. This is a direct consequence of the FLT (First Law of Thermodynamics):

$$P_{delivered} = G_{net}\ c_P \cdot (T_{sup} - T_{ret}) \quad [MW]$$

Even though the influence of such perturbations on T_{ret} should be thoroughly investigated, it might be assumed that the lower T_{sup} is, the higher the compensation operated by the mass-flow rate should be, and so would be the pumping duty of the centralized plants. A second issue might also arise from fluid-dynamic overload, i.e. the presence of considerably high amounts of water flowing in the conduits, which are beyond the maximum, acceptable value set by the geometrical dimensions of the pipes themselves, thus giving birth to undesired fluid-dynamic perturbances.

The problem may be smartly tackled by introducing TES (Thermal Energy Storage)s in purposely chosen points of the District Heating Network: TES are large reservoirs of hot water, whose aim is backing up the plant(s) as soon as the heating systems of the end-users are switched on, especially when the power demand peaks during the first hours in the morning. They are filled with hot water at night, i.e. when the demand is close to null, making them an intelligent and valid way to address the problem of centralized overload.

This work focuses on analyzing how the number, size and position of storages in an existing DHN influences the thermal load at the central plant, if lower supply temperatures were chosen.
A numerical model of the Thermal Energy Storage has been developed and integrated into the simulation of the network. After a brief overview and explanation regarding how the study of DHNs is usually carried out, the reader may find a detailed description of the numerical model of the storage itself. In the next section, the problem of the network with a lower supply temperature is investigated before

carrying out several tests, in order to infer how the storages affect the performances of the network itself.

Chapter 2

The Numerical Model of the Network

2.1 Preliminary Considerations

The following study relates to a portion of the distribution network of Turin, the schematic of which is illustrated below.

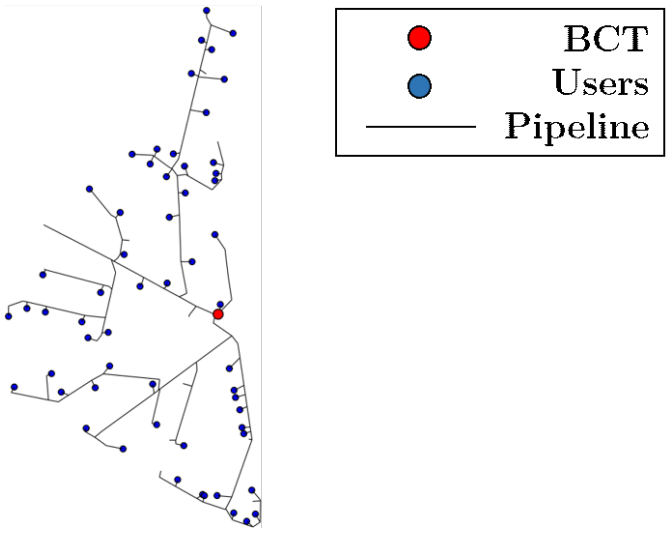

Figure 2.1: One dimensional representation of the Network.

Blue dots represent the end-users, while the red one indicates the point, from which hot water is injected into the pipeline. Since that the object of this work is a small distribution network, the point that has been labelled as BCT – which stands for *barycentric* node – in Fig. 2.1 actually indicates the junction between the latter

and the upstream transportation pipeline, rather than being an actual central heat production facility.

Performing a complete and detailed analysis of a District Heating Network means to compute the mass-flow rate, pressure and temperature distributions along the pipes and at every junction. Therefore, even at first glance, it is noticeable that a thorough study of such system would be extremely complicated and time-consuming.

On the other hand, it might also be observed that the geometrical characteristics of the network itself may enable to adopt a simplified, one-dimensional approach. In fact, once having indicated with L the length of the pipes, and with D their diameters, it could be safely stated that $L >> D$, as water conduits are from a few to several kilometers long, whereas diameters are in the order of hundreds of centimeters.

From the physical point of view, this leads to the following assumption, i.e. the variation of the fluid properties in the two directions orthogonal to the flow is by far negligible, with respect to the meridian one. In other words, the thermal and fluid-dynamic analysis of the whole network may be restricted to the axial direction of the water stream only.
The computational implications linked to the adoption of a one-dimensional model, as well as a more detailed description of the latter are illustrated in the following section, and are based on the contents of [9].

2.2 The One-Dimensional Model

2.2.1 The Topology of the Network

The study of a District Heating Network, as performed exploiting the 1D approximation, deeply relies on the use of graph theory. In fact, thanks to the introduction of a few, simple concepts, it enables the user to rapidly model and investigate the topology of the network, i.e. how its junctions are interconnected, as well as to take into account the presence of additional items, such as pumps and/or fans placed all along the pipeline.

The two main elements of graph theory one should immediately familiarize with are *nodes* and *branches*:

- A *node* is basically a junction, hence a point to which one or more pipes are linked. State variables - for instance mass, pressure and temperature - are defined in nodes.

- A *branch* is an oriented line, bounded by two nodes.

  For what the study of District Heating networks is concerned, branches are nothing but the 1D representation of water pipes. Hence, their complete definition takes in also the geometrical and physical properties of the pipes themselves, such as their lengths, diameters, conductivity, etc.

For the purpose of unambiguously describing its topology, it is important that nodes and branches are numbered, before building the so-called *incidence matrix* $\underline{\underline{\mathbf{A}}}$. This item is composed of a number of rows equal to the number of nodes, and as many columns as the branches. The elements of $\underline{\underline{\mathbf{A}}}$ can easily be filled, taking into consideration that:

- $A_{i,j} = 1$, if the $i-th$ node is the inlet (upstream) node of the $j-th$ branch.
- $A_{i,j} = -1$, if the $i-th$ node is the outlet (downstream) node of the $j-th$ branch.
- $A_{i,j} = 0$, else.

Basically, the incidence matrix immediately shows whether a stream is moving according to the positive-chosen direction or not.

2.2.2 The Fluid-Dynamic Problem

The following step to take towards the solution of the network consists in solving the fluid-dynamic problem, i.e. solving the *continuity equation* (2.1) and the *momentum balance* (2.2), to find the pressure and velocity (i.e. the mass-flow rate) distributions in the nodes and the branches, respectively.

$$\frac{\partial \rho}{\partial t} + \nabla \cdot \rho \underline{\mathbf{v}} = 0 \tag{2.1}$$

$$\rho \frac{D\underline{\mathbf{v}}}{Dt} = -\nabla p - \nabla \cdot \underline{\boldsymbol{\tau}} + \underline{\mathbf{F}} \tag{2.2}$$

For what the present case study is concerned, the problem actually shrinks to the solution of the following linear system of equations only, which is nothing but the matrix form of the *continuity equation*, built upon cleverly exploiting the structure of the incidence matrix.

$$\underline{\underline{\mathbf{A}}} \cdot \underline{\mathbf{G}} + \underline{\mathbf{G}}_{ext} = \underline{\mathbf{0}} \tag{2.3}$$

where:

- $\underline{\mathbf{G}}$ is the vector of the NB unknown mass-flow rates, where NB indicates the number of branches.

$$\underline{\mathbf{G}} = \begin{Bmatrix} G_1 \\ G_2 \\ \vdots \\ G_j \\ \vdots \\ G_{NB} \end{Bmatrix}, \quad j = 1, 2, \ldots, NB$$

- $\underline{\mathbf{G}}_{ext}$ is the vector of injected and/or extracted mass-flow rates into/from the NN nodes of the network. According to the definition of A, $G_{ext,i} < 0$ if the flow is extracted from a node, vice-versa if injected. It is worth underlining that these quantities represent the boundary conditions of Eq. 2.3 itself.

$$\underline{\mathbf{G}}_{ext} = \begin{Bmatrix} G_{ext,1} \\ G_{ext,2} \\ \vdots \\ G_{ext,i} \\ \vdots \\ G_{ext,NN} \end{Bmatrix}, \quad i = 1, 2, \ldots, NN$$

Solving equation 2.3 is enough to obtain the whole fluid-dynamic scenario of the network, since that the latter is tree-shaped, i.e. without any closed loops. In other words, the solution of the *continuity equation* immediately provides the user with the correct values of the mass-flow rates. If the network had one or more closed loops, a different - and more complex - approach should be followed to handle the pressure-velocity coupling, thus to simultaneously compute both mass-flows in the branches and nodal pressures.

2.2.3 The Thermal Problem

The thermal problem concerns the solution of *energy conservation* equation.

$$\rho \frac{Du}{Dt} = -\nabla \underline{\mathbf{q}} - p\nabla \cdot \underline{\mathbf{v}} - \underline{\boldsymbol{\tau}} \colon \nabla \underline{\mathbf{v}} \tag{2.4}$$

Solving this equation would yield the temperature field in every point of the computational domain. However, since that there exists no analytical, exact solution of the latter, a proper discretization scheme should be applied to convert Eq. 2.4 into a system of algebraic equations. A Finite Volumes method has been

applied here: its working principle consists in dividing the domain into arbitrarily small control volumes - called cells. Each cell is then assigned a representative value of the unknown variable, i.e. its value in the center, while surface quantities are approximately evaluated at the boundaries. It should be emphasized that there are different strategies and numerical schemes available to do so, each of which yields more or less acceptable results, according to the nature of the computational problem. For what the present case study is concerned, the upwind scheme has been selected. If the fluid-dynamic problem has been solved, i.e. if the directions of the flows in every branch are already known, the scheme works as depicted below.

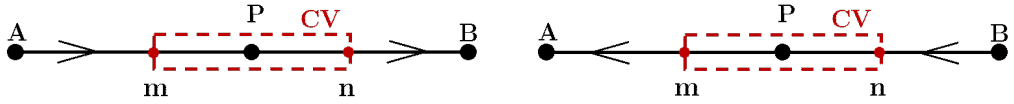

(a) Upwind Scheme 1. **(b)** Upwind Scheme 2.

Figure 2.2: How the Upwind Scheme works.

Having labelled with m and n the cell boundaries and indicating with x a generic unknown:

- $x_m = x_A$ and $x_n = x_P$, if the flow goes from A to B.
- $x_m = x_P$ and $x_n = x_B$, if the flow goes from B to A.

For what this case study is concerned, the control volume to which the Finite Volumes discretization is applied is illustrated in Fig. 2.3. The unknown, cell center values are the temperatures $T_i,\ i = 1, 2, \ldots, NN$ evaluated at the NN junctions. In a similar way to what has been done with the *continuity equation*, a simplified version of equation 2.4 may be written for the one dimensional case, at the $i - th$ junction.

$$\frac{\partial}{\partial t}(\rho c_P T_i)\Delta V + \sum_{j}^{NB}(\rho v_{ax} S)_j c_p T_j = k\frac{\partial T}{\partial x}\bigg|_j S_j - \Phi_L \tag{2.5}$$

The first term of 2.5 consists in the rate of change of total energy in the CV, with T_i being the temperature of water in the junction. The second term represents the advective fluxes of energy entering or exiting the node – with temperatures T_j being evaluated (actually approximated by the upwind scheme) at the CV boundaries – while the first contribution on the RHS stands for the (negligible) conductive term. Φ_L accounts for thermal losses between the branch and the external environment.

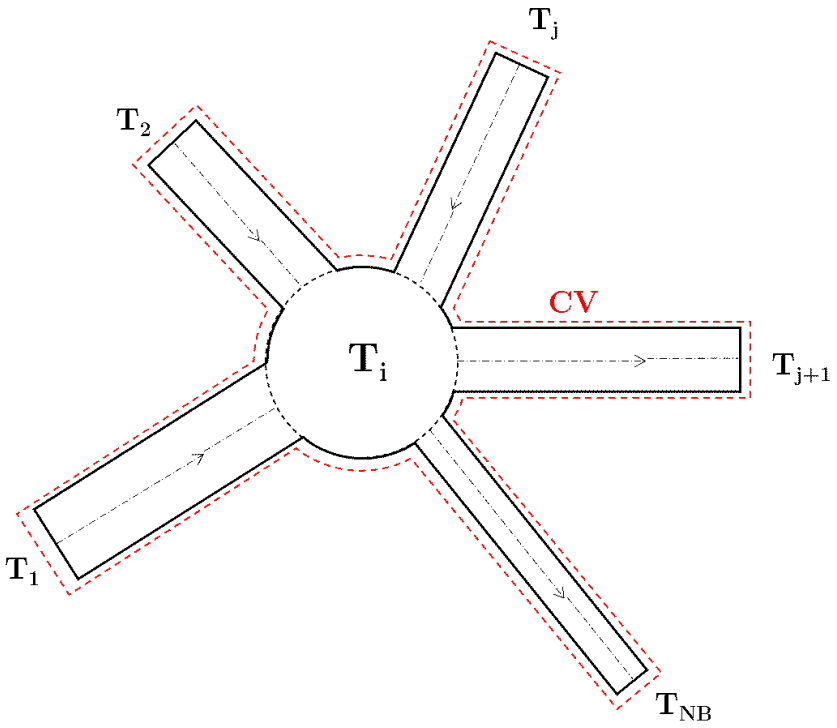

Figure 2.3: Control Volume adopted for the Thermal Problem.

Two further assumptions have been made:

1. Perfect and adiabatic mixing is assumed, i.e. every outgoing water stream has the same temperature T_i.

2. Thermal losses are proportionate to the temperature difference between the junction and the ground:

$$\Phi_{L,i} = \sum_{j}^{NB} \frac{L_j}{2} \pi D_j U_j (T_i - T_g) \tag{2.6}$$

   where U_j and T_g are the global heat transfer coefficient of the $j-th$ branch and the ground temperature, respectively.

The set of nodal equations 2.5 can be cast into the following system of linear equations, to be solved at every time instant Δt:

$$\left(\underline{\underline{\mathbf{M}}} + \underline{\underline{\mathbf{K}}}\right) \cdot \underline{\mathbf{T}}\,(t) = \underline{\mathbf{f}} + \underline{\underline{\mathbf{M}}} \cdot \underline{\mathbf{T}}\,(t + \Delta t) \tag{2.7}$$

where $\underline{\underline{\mathbf{M}}}$ is called *mass matrix*, $\underline{\underline{\mathbf{K}}}$ *conductance matrix*, and $\underline{\mathbf{f}}$ is the vector of known terms.

2.3 A First Glance on Numerical Results

Once the computational setup has been completed, the thermal fluid-dynamic simulation of the network may be carried out.

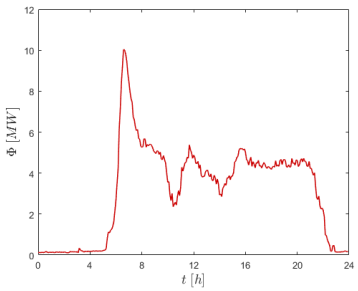

Figure 2.4: Thermal load.

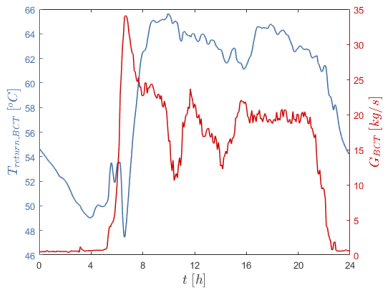

Figure 2.5: Mass-flow rate and T_{ret}.

Figure 2.4 illustrates how the thermal load at the *barycentric* node varies during a day in January. It is noticeable that during the first hours in the morning there is a sharp increase in the load profile, to cope with the sudden rise in the heat demand by the users, but most of all to compensate for the low supply temperature of water, which is subject to considerably longer transients, with respect the fluid-dynamic ones.
A graphical representation of this phenomenon is shown in Figure 2.6: at $07:15$ the mass-flow rate demand has already peaked. However, most of the network is still at a relatively low temperature. On the contrary, it may be observed how hotter it is a little more than one hour later, with the majority of the users that are being delivered water at a temperature almost as high as T_{sup}.
During the rest of the day instead, the changes in the load are subtler, and the behavior of the network resembles the one depicted in figure 2.6b. It is also worth noticing that during the course of night hours the thermal load is slightly more than null, a sign that there are some users with a nightly demand, e.g. hospitals.

Even intuitively, the mass-flow rate injected into the network shows the exact same pattern of the thermal power, whereas a different, almost mirrored behavior is experienced by the return temperature of water. This figure is the natural outcome of all the mixing processes happening along the pipelines of the return circuit, and is one of the most important performance indicators of the network.
In fact, recalling the *FLT* to express the power exchanged at the central node:

$$P_{BCT} = G_{DHN} \cdot c_P \cdot (T_{sup} - T_{ret})$$

it is plain to see that – once T_{sup} is fixed by the production facility and since that the specific heat of water is constant for a prescribed temperature – obtaining a

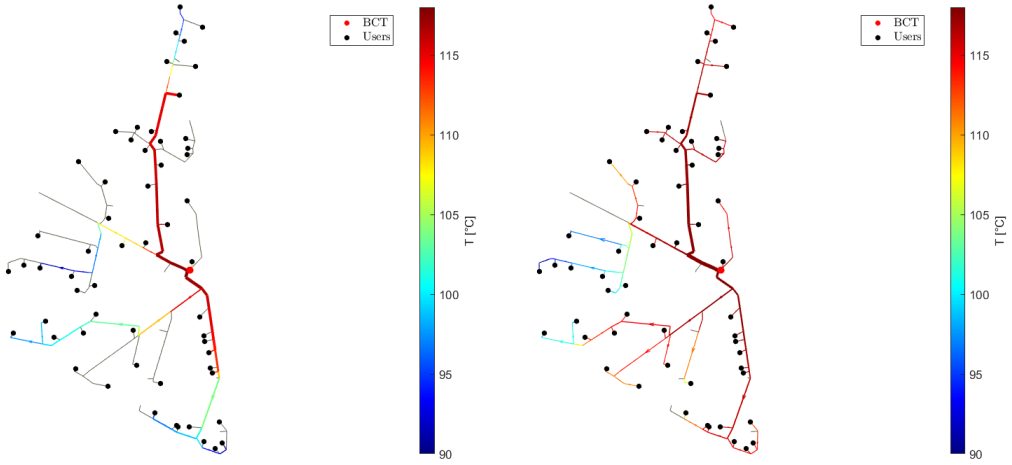

(a) Temperatures of the Network at 07 : 15 **(b)** Temperatures of the Network at 08 : 30

Figure 2.6: Temperatures in the network at two moments in the morning.

lower T_{ret} after having exchanged an equal amount of power, means that fewer water has been pumped into the network, hence reducing the pumping costs and increasing the overall efficiency of the network.

Chapter 3

The Thermal Energy Storage

3.1 How Thermal Energy Storages work

In the field of District Heating systems, a Thermal Energy Storage (TES) can basically be regarded as a heat capacitor that periodically stores and discharges thermal energy.
These accumulators may be classified into a wide range of categories according, for instance, to the way they stock and release energy or their characteristic charge and discharge times [10]. In this work sensible heat and short-term storages are considered, i.e.large, thermally insulated and pressurized tanks that behave according to the following two-step process [11]:

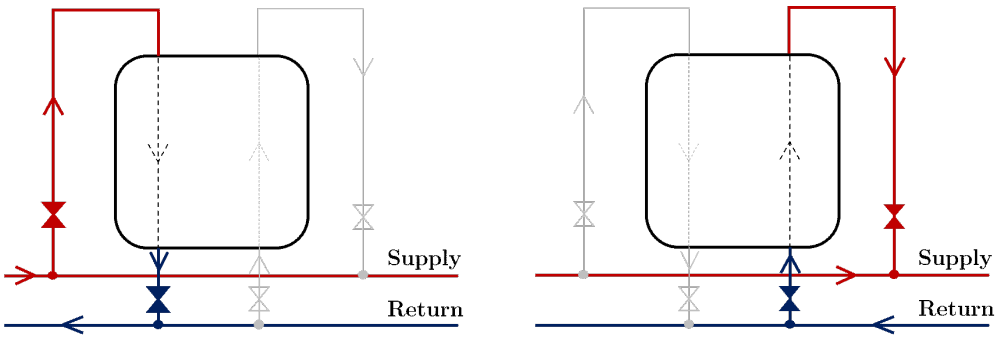

(a) Charging Phase. **(b)** Discharge Phase.

Figure 3.1: How the Thermal Energy Storage works.

- During the course of night hours the *charging* phase occurs: exploiting the

little heat demand of the whole network, hot water is produced at the central plants and conveyed into the storages. At the same time, the cooler fluid that had been filling the tank up to that moment gets re-injected into the return circuit.

During this period then, the TES behave exactly as an end-users would do.

- As soon as the heating systems are turned on, the *discharge* begins: the hot water stocked into the reservoirs is pumped into the pipelines, towards the end-users. Conversely, water coming from the return network starts filling the tanks.

  In this case, the TES act as ancillary central plants.

3.2 Numerical Model of the TES

3.2.1 Proper Sizing

A numerical model of the storages has been developed and integrated into the simulation of the network. In accordance with graph theory, the insertion of one or more reservoirs has been modelled adding an equal number of both extra branches and nodes. Prelimirarily though, they should be consistently designed, so that they can comply with the constraints of the network.
To begin with, the storage has been assigned an equal and hypothetical capacity – in terms of m^3 of storable water – that has been converted into a correspondent value of energy. Subsequently, the intervals during which the charging and discharging phases occur are chosen; in the following sections, they are labelled with Δt_{ch} and Δt_{dis}, respectively.
After these brief setup operations, three feasibility checks are carried out.

1. During the charging phase, the water mass-flow rate that fills the storage must be less than the the maximum admissible value for the branch upstream of the junction, to which the storage is connected. With reference to figure 3.2, this means that the inequality

   $$G_{charge} + G_{users} \leq G_{th} \tag{3.1}$$

   must be satisfied, for any instant during Δt_{ch}.

   The threshold value G_{th} depends on the diameter of the pipe and on the maximum admissible flow velocity, according to continuity:

   $$G_{th} = \rho \cdot A_S \cdot v_{max} = \rho \cdot \frac{\pi D_{branch}^2}{4} \cdot v_{max}$$

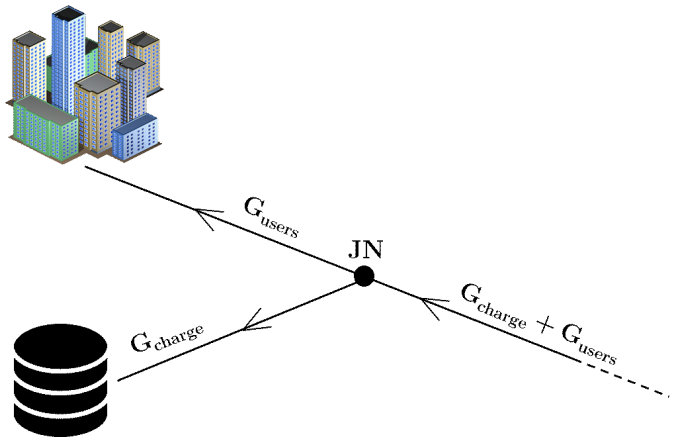

Figure 3.2: Mass-Flows during the charging phase.

where $v_{max} = 0.7\ m/s$.

G_{charge} is computed applying the FLT during the charging interval:

$$G_{ch} = \frac{Energy}{c_P \Delta t_{ch}} \left(\overline{T}_{sup}(t) - \overline{T}_{ret}(t)\right) \tag{3.2}$$

where $\overline{T}_{sup}$ and $\overline{T}_{ret}$ are the average supply and return temperatures evaluated at the junction node, during Δt_{ch}. If the boundary condition 3.1 is not met, a larger Δt_{ch} is selected. It should be marked that a lower bound for Δt_{ch} has been set, corresponding to $22:00$ o' clock of the previous day.

If 3.1 is not satisfied even with the largest available time interval, the size of the storage is progressively reduced, until a proper value of G_{ch} is obtained.

2. During the course of the discharge phase, the overall flow-rate pumped from the storages into the network at every instant must be lower than the correspondent amount that the plant would inject, if there were not any reservoirs. In fact, if this happened, there would be extra water that could flow nowhere but towards the *barycentric* node, however this would not be physically consistent.

   The condition to be satisfied is then:

$$\sum_{i=1}^{N_{TES}} G_{inj,i}(t) \leq G_{BCT}(t) \tag{3.3}$$

3. The third and last boundary condition to be met regards once again the discharge phase. When the water is injected from the storage into the pipelines, two things may happen. With reference to the Fig. 3.3:

- The amount of injected water $G_{discharge}$ is not sufficient to satisfy the demand of the users located downstream the junction node JN, therefore the storage must be backed up by the central plant.
- The injected mass-flow rate is larger than the one required by the users located downstream the junction node, hence the supplementary portion of water will leave JN flowing in the opposite direction. Similarly to what has been illustrated in the first boundary condition, this means imposing

$$G_{discharge} - G_{users} \leq G_{th} \tag{3.4}$$

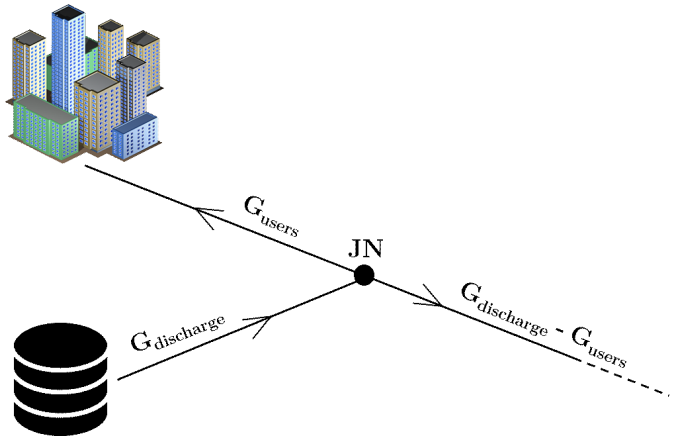

Figure 3.3: Division of the mass-flow rate during the discharge.

Eventually, the size of the storages will be consistent with the fluid-dynamic constraints of the network.

3.2.2 Modification of the Model of the Network

As briefly mentioned in the previous section, the presence of one or more storages has been modelled adding N_{TES} extra nodes – corresponding to the TES themselves – and an equal number of supplementary branches, connecting the first ones to the already existing network.
The diameters of the branches have been computed - once again - on the basis of the maximum admissible flow velocity: after calculating the so-called *theoretical diameter*:

$$D_{th} = \sqrt{\frac{4 \cdot G_{TES_{max}}}{\pi \rho v_{max}}} \quad [m]$$

The actual cross-section of the pipe has been selected among the standard dimensions for water pipes, available on the market.
The length of the conduits has been arbitrarily set to 1 m.

Further on, the *incidence matrix* has to be properly modified, to account for the introduction of the TES. An N_{TES} number of rows and columns has been added, as illustrated in the following figure:

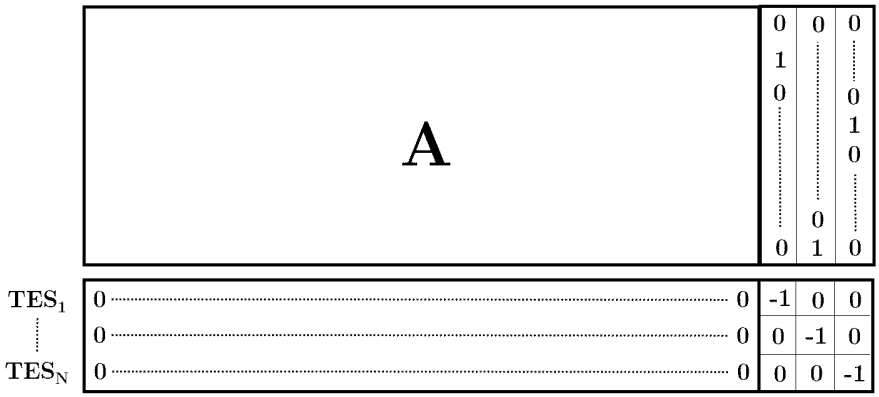

Figure 3.4: Modified Incidence Matrix.

It is worth pointing out that the rows corresponding to the nodes of the storages have only one non-null element, because they may behave either as a central plant, or as an end-user, as already mentioned in Sec.3.1.
In a similar way, the boundary conditions of the *continuity equation* have been updated. In fact, the vector

$$\mathbf{G_{ext}} = \begin{Bmatrix} G_{ext,1} \\ G_{ext,2} \\ \vdots \\ G_{ext,i} \\ \vdots \\ G_{ext,NN} \end{Bmatrix}, \quad i = 1, 2, \ldots, NN$$

has been added N_{TES} rows, each of which contains the time-dependent vector of mass-flow rates incoming and leaving the storages (see Fig. 3.5).
To complete the setup of the model, and be ready to run the simulation of the network, the boundary conditions for the solution of the thermal problem have to be imposed.

- While charging, the storage plays the role of an end-user: it gets delivered water from the supply circuit according to its demand, and at the same time

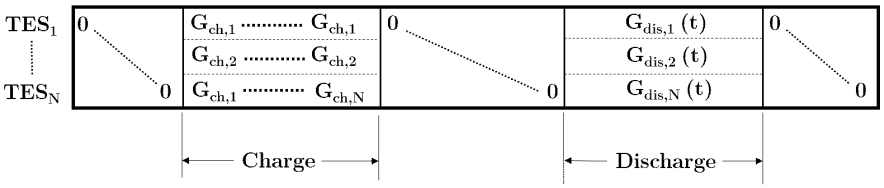

Figure 3.5: Modified Vector of Boundary Conditions.

it injects the fluid stored during the previous day into the return pipelines. However, while the temperature of the water leaving a substation and flowing through the return network varies according to the thermal load profile of its specific user, in the case of the TES – in which there is no heat exchanger – it may be assumed to be constant, and equal to the average of the values that had been filling the tank during the discharge phase of the day before:

$$T_{dis} = \frac{1}{N_{samples}} \cdot \sum_{i=1}^{N_{samples}} T_{ret}\left(t_i\right) \tag{3.5}$$

where $N_{samples} = \dfrac{\Delta t_{dis}}{\Delta t_s}$ is the number of sampled values during Δt_{dis}, with $\Delta t_s = 60\ s$ being the sampling period.

Actually, this assumption is valid, as long as buoyancy effects and thermal stratification are neglected [1].

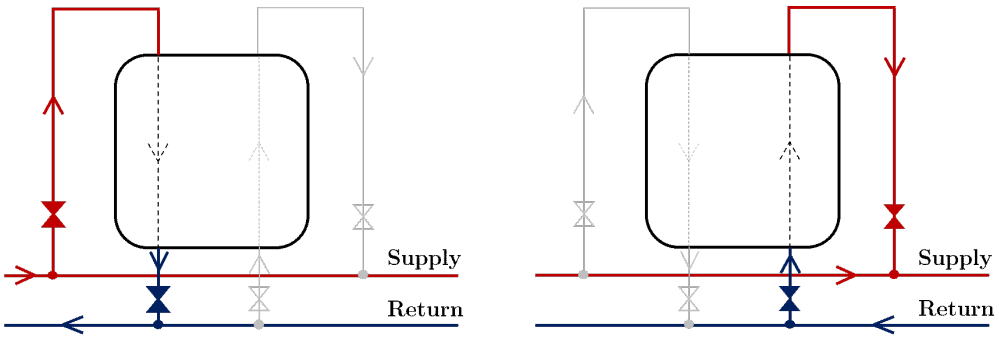

(a) Charging Phase. **(b)** Discharge Phase.

Figure 3.6: Boundary Conditions for the Thermal problem.

- Throughout the discharge phase instead, the storage works like the central plant, hence it pumps water into the supply circuit at a prescribed temperature. In a way similar to Eq.3.5, its value has been computed averaging the the

supply temperatures during the time frame of the charge:

$$T_{ch} = \frac{1}{N_{samples}} \cdot \sum_{i=1}^{N_{samples}} T_{sup}\left(t_i\right) \tag{3.6}$$

with $N_{samples} = \dfrac{\Delta t_{ch}}{\Delta t_s}$ being this time the number of sampled values during the course of the charging phase.
After these last two steps, the model of the Thermal Energy Storage is completed and ready to be integrated into the numerical simulation of the network.
It is worth observing how the introduction of a storage influences the behavior of the central plant, in terms of both the fluid-dynamic and the thermal load, even in the case of the design supply temperature, i.e. $T_{BCT} = 118\ ^oC$.
The experimental data adopted throughout the computations has been provided by *IREN S.p.A.*, i.e. the company in charge of managing the DH network of Turin, for three whole heating seasons, from year 2015 to 2017.

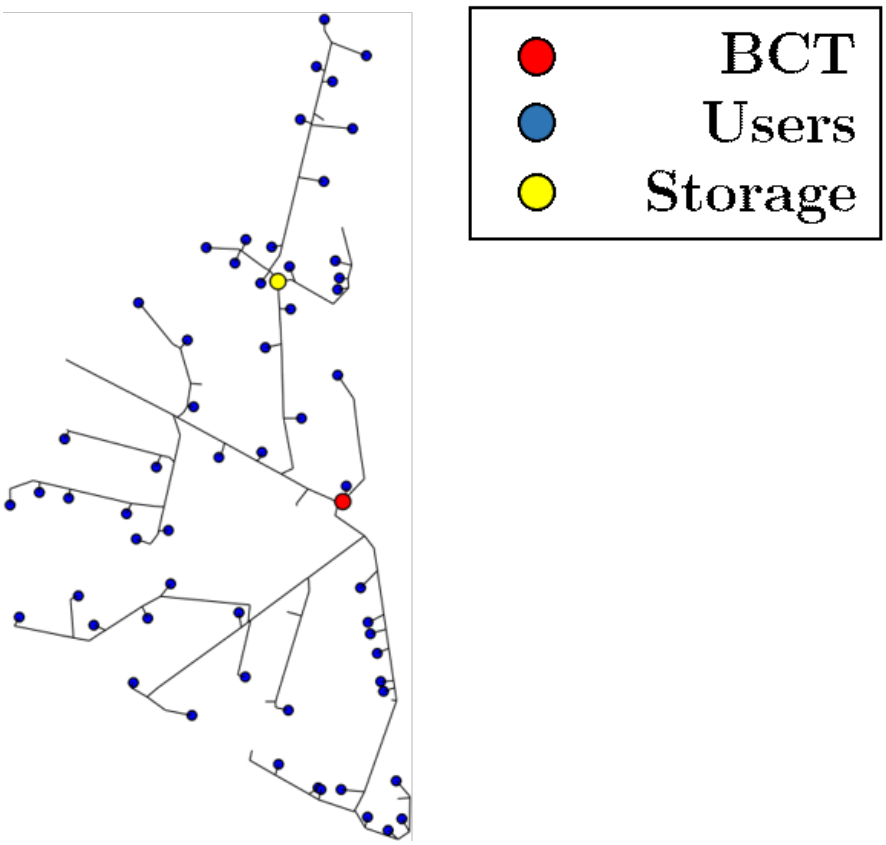

Figure 3.7: Position of the Storage.

A storage with capacity $V_{stor} = 50\ m^3$ has been positioned in correspondence of the yellow dot of Fig. 3.7. As it might have been expected, its introduction made the peak value of thermal power decrease, passing from more than 10 MW to a little more than 8 MW (Fig. 3.8a). In the left lower corner of the same picture, the augmented thermal load during the charging phase can be observed.
A mirrored behavior characterizes the pumping duty, represented in Fig. 3.8b.

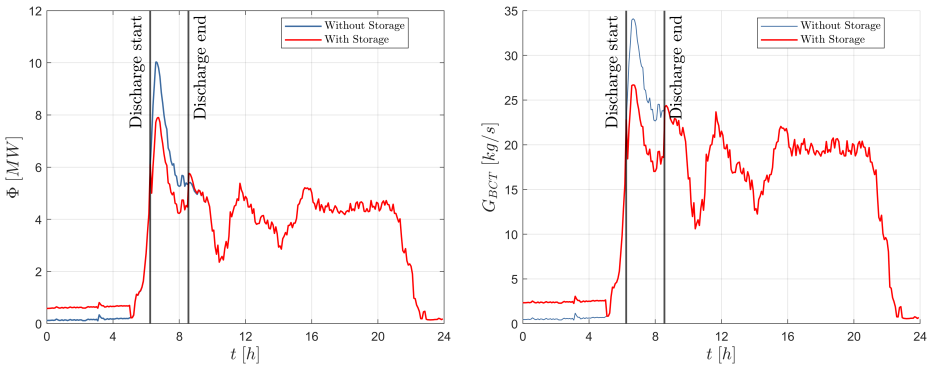

(a) Thermal Load with and without the storage.

(b) Fluid-Dynamic Load with and without the storage.

Figure 3.8: Influence of the introduction of one $V_{stor} = 50\ m^3$ Storage.

Chapter 4

The Network in Off-Design Conditions

4.1 Thermal and Fluid-Dynamic aspects

The main aim of this work consists of finding the best combination of the position and size of one (or more) Thermal Energy Storages in a District Heating Network, in order for the central plant to not be subject to an unacceptable overload – in terms of pumping duty – if the temperature of the supplied water were lowered. These insights have already been discussed in the very first pages of this report. However, in this chapter a deeper and more detailed analysis is going to be carried out, to gain a more accurate understanding of the consequences that the aforementioned temperature reduction brings about.

In order to deliver the required amount of power to every user when hot water is pumped at a lower temperature, all the substations must be flown through by a larger mass-flow rate. Therefore, the first step towards the study of the DHN in off-design conditions is the computation of their new, augmented fluid-dynamic load.
In steady-state conditions, the following energy balance may be applied across the heat exchangers:

$$\Phi_{network} = G_{network} c_P (T_1 - T_2) = G_{user} c_P (T_3 - T_4) = \Phi_{user} \tag{4.1}$$

where T_1 and T_3, and T_2 and T_4, are the supply and return temperatures of the water, on the network and user side, respectively (see also Fig.4.1).

Eq. 4.1 yields reliable results only in steady-state conditions, i.e. relatively far from the instants, in which the heating systems of the users are switched on. In order to

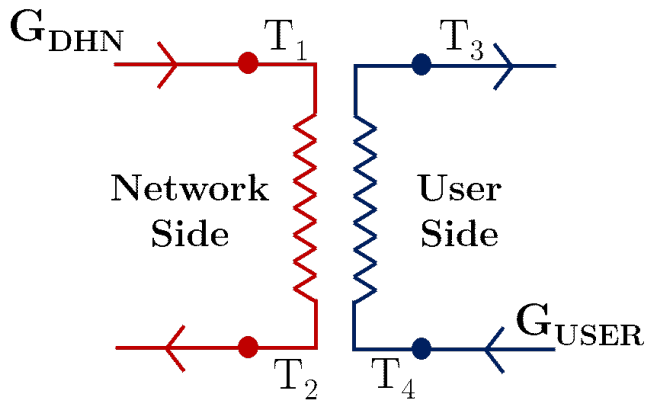

Figure 4.1: Schematic of the Heat Exchanger of a SST.

handle these thermal transients appropriately, a term accounting for the effects of the high thermal capacity of the hot water should be included in the formulation of the energy balance. However, this phenomenon has not been considered here, since that it is not the main purpose of this work.

Additionally, it is worth highlighting that the quantity at the *LHS* of the equation would be always slightly higher than the product on its *RHS*, due to thermal losses occurring inside the heat exchanger. In other words, the power absorbed by the secondary side of the substation is a little lower, with respect to the actual thermal flow that the primary stream would deliver, if such losses were not present. On the other hand, this difference is so little that it may safely be neglected, with satisfactory approximation.

4.1.1 Analysis of the Substations in Off-design Conditions

In this section, the procedure followed to perform the analysis of the substations in off-design conditions is illustrated. Prior to the explanation though, it is worth making a brief premise, concerning how the control system of a District Heating substation works [4].

The control loop starts by measuring the outdoor temperature, from which the so-called *set-point* temperature T_{sp} is computed: this is the temperature at which the water stream entering the space heating terminals should be, in order to ensure the right room temperature in the building. Depending on the difference between the actual water temperature and the prescribed T_{sp}, an actuator regulates the stroke of a valve placed along the return circuit on the primary side, hence increasing or

reducing the mass-flow rate coming from the DH network.
If the supply temperature of the DH network is reduced, two scenarios are possible, at the substation level. With reference to Figure 4.1:

- Even if T_1 is lower than design conditions, the reduction is small enough, to be compensated by the rise in mass-flow rate. From a real perspective, this means that it is still possible to guarantee the *set-point* conditions, in terms of T_3 and delivered power. Consequently, the supply temperature of the network may be lowered even more.
- The temperature reduction is too harsh to be handled by the substation, meaning that the control system has made the mass-flow rate surge up to its threshold value G_{th}, but even so the measured value of T_3 is not close enough to T_{sp}. Therefore, a smaller amount of power would inevitably be delivered to the building, thus forcing the room temperature inside the building to be lower than the desired value.

In the following sections, the results of several simulations that have been run considering the first of the two scenarios listed above, are going to be displayed.
For what the computation of the off-design mass-flow rate demands is concerned, an iterative procedure has been developed, exploiting the *FLT* and the so-called ε - *NTU* method for the analysis of off-design performance of heat exchangers [12]. Basically, the iterative loop revolves around the concept of effectiveness itself: this is defined as the ratio between the actual exchanged power and the maximum potentially exchangeable power. With reference to Fig. 4.1:

$$\varepsilon_{exp} = \frac{P_{actual}}{C_{min} \cdot (T_1 - T_4)} \tag{4.2}$$

where subscript *exp* emphasizes the fact that the expression may be computed substituting experimental, i.e. measured data, into the equation. The quantity C_{min} corresponds to the minimum thermal capacity, between the two fluids flowing through the heat exchanger:

$$C_{min} = min(c_{P_{net}} \cdot G_{net},\ c_{P_{user}} \cdot G_{user}) \quad \left[\frac{W}{K}\right] \tag{4.3}$$

Actually, since that in this case there is water flowing on both sides of the heat exchanger, Eq. 4.2 may be simplified to the following expression:

$$\varepsilon_{exp} = \frac{P_{actual}}{c_P \cdot min(G_{net},\ G_{user}) \cdot (T_1 - T_4)} \tag{4.4}$$

Eq. 4.2 may be regarded as the operative definition of the effectiveness, in the sense that it is always valid, regardless of the geometrical properties of the heat

exchanger. However, it is also possible to express ε as a function of the so-called number of transfer units and the heat capacity ratio, being them respectively:

$$NTU \coloneqq \frac{U \cdot A_S}{C_{min}} \tag{4.5}$$

$$c = \frac{min(G_{net},\ G_{user})}{max(G_{net},\ G_{user})} \tag{4.6}$$

The analytical formulation involving these two quantities is, on the contrary, dependent on the shape and type of the heat exchanger. The ones installed in District Heating substations are usually plate heat exchangers (PHEX), a schematic of which is illustrated below:

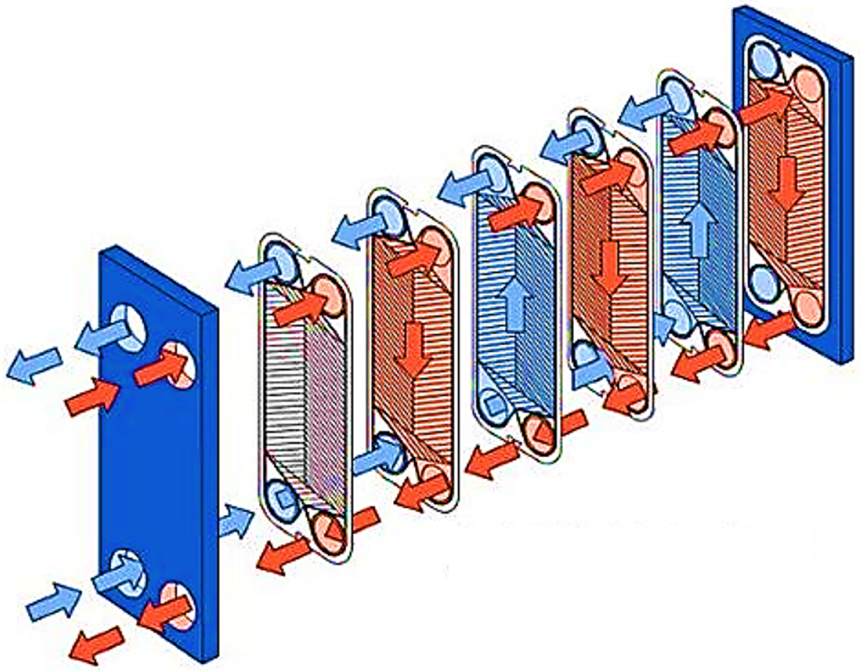

Figure 4.2: Scheme of a PHEX[1].

Basically, these devices are made of a set of thin metal plates packed together by means of bolts that are clamped to the end plates (the two thicker ones in the figure). The hot and cold water streams flow alternatively within the channels, thus enabling the heat exchange to occur. The geometry of the plates is significantly

[1]Source: alfalaval.com

complex and purposely designed for every application, to ensure that heat transfer is the most effective, thus it may be different even from one heat exchanger to another [13]. Nonetheless, it is possible to model its behavior, with remarkably satisfactory approximation, considering it as a counter-current, double-pipe heat exchanger:

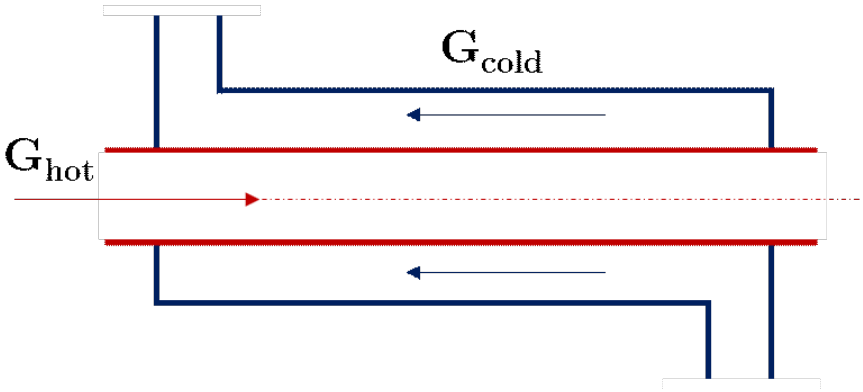

Figure 4.3: Double Pipe Heat Exchanger.

This simplification may be justified, even intuitively, by observing that despite the overall complexity of the plate heat exchanger, the pattern of the streams flowing within the channels is extremely close to the one depicted above.
The expression of the effectiveness for the double-pipe counter-current heat exchanger is the following:

$$\epsilon = \varepsilon(NTU, c) = \frac{1 - e^{-NTU(1-c)}}{1 - c \cdot e^{-NTU(1-c)}} \tag{4.7}$$

Before illustrating how the off-design mass-flow rates on the primary sides have been computed, it is worth making a further premise, regarding the values of flow-rates on the users' ones.
As previously mentioned, these are the water streams that flow through the heating terminals of every specific user, e.g. radiators, floor heating panels and fan coils, and could easily be calculated by applying FLT across the heat exchanger:

$$G_{user}(t) = \frac{P(t)}{c_P \cdot (T_3(t) - T_4(t))} \quad \left[\frac{kg}{s}\right] \tag{4.8}$$

Even though the values of G_{user} should be constant for every substation, the actual results of Eq. 4.8 show a fluctuating behavior, mainly because of the measurement errors occurring when the two temperatures on the secondary side are detected by the control system. It should be highlighted though, that these values always

oscillate around a mean quantity, hence a set of constant values has been determined and adopted throughout this work, following a two-step, stochastic-driven approach:

1. The probability distribution functions of the values of the time-series have been computed, in order to detect and discard possible outliers.
2. Every substation has been assigned a value of G_{user}, equal to the average of the remaining numbers.

Once the amounts of water flowing at the secondary sides of the substations have been obtained, it is possible to solve the problem of the off-design mass-flow rates. The core of the algorithm consists of expressing the heat flux exploiting both the FLT – applied on the primary side of the heat exchanger – and the definition of the effectiveness:

$$P^* = G_{net}\, c_P \cdot (T_{1_{off}} - T_2) \tag{4.9}$$

$$P^* = \varepsilon c_P \cdot min(G_{net},\ G_{user}) \cdot (T_{1_{off}} - T_4^*) \tag{4.10}$$

where:

- P^* is the design value of the power, that must be ensured in off-design conditions.
- $T_{1_{off}}$ is the supply temperature on the primary side in off-design conditions, which is known after the simulation of the network has been run.
- T_4 is the design value of the return temperature, on the user side.

According to the provided data, the network mass-flow rate is actually always lower than the correspondent value of G_{user}, therefore it may be assumed that there exists, for a known value of $T_{1_{off}}$, a combination of G_{net} and ε that simultaneously satisfies 4.9 and 4.10. The algorithm aims at finding this couple of values, for every time instant.
First of all, the design value $G_{des}(t^*)$ of mass-flow rate at a time t^* is augmented by an arbitrarily small quantity dG, yielding the tentative value $G_{guess}(t^*)$. Then, a vector of guessed thermal fluxes $P_{guess}(t^*)$ is computed, for different values of ε – ranging from 0 to 1. FLT is applied on the secondary side of the substation, to calculate the vector of $T_{3_{guess}}(t^*)$ quantities, whose closest value to the one of design conditions T_3^* is extracted, together with its correspondent $P_{guess}(t^*)$. If the latter is close enough to the design value $P_{des}(t^*)$, i.e. if their difference is less than a prescribed tolerance, the algorithm stops, otherwise $G_{guess}(t^*)$ is again increased by dG. Figure 4.4 displays the flow diagram of the whole algorithm, providing a graphical and more comprehensible representation of the whole picture.

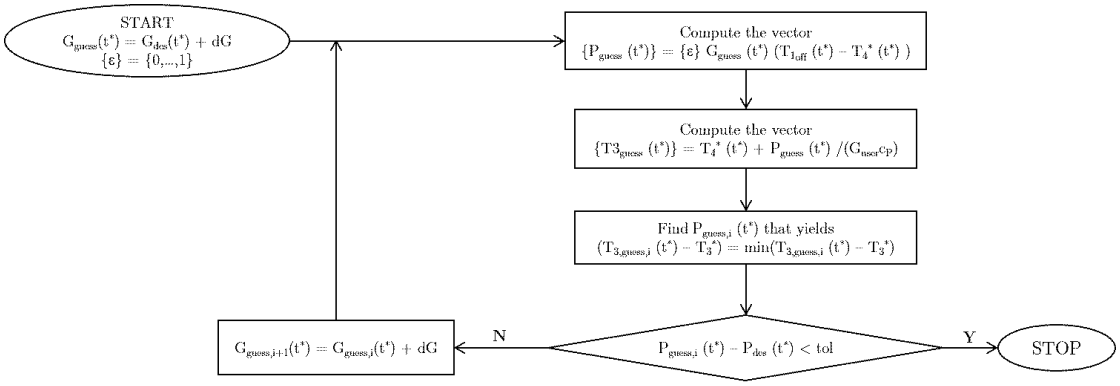

Figure 4.4: How to compute off-design mass-flow rates.

Chapter 5

Analysis of the Results

In this section, several tests have been conducted, in order to detect the factors that influence the performances of the DH network, when the supply temperature is reduced and, at the same time, the storages are added. Their effectiveness has been analyzed observing how much they can reduce the maximum load at the central plant level. In other words,

$$P_{max} = max(P_{BCT}(t)) \tag{5.1}$$

is the objective function that has been monitored, with the purpose of minimizing it.
Results have been observed upon choosing three different sizes, i.e. 25 m^3, 50 m^3, and 75 m^3, corresponding to roughly 5000 MJ, 10000 MJ and 15000 MJ of storable energy.
All the calculations, as well as the results illustrated in the following pages, have been respectively carried out and extracted working with the software *MATLAB*.
Additionally, in the plots that are going to be illustrated:

- Design conditions refer to a supply temperature of $T_{BCT} = 118^o\ C$.
- Off-design conditions are instead related to the network with reduced supply temperature, and in which the reservoirs have been introduced. A new $T_{BCT} = 114\ ^oC$ has been adopted, all throighout these tests.
- The charging phase lasts from 22 : 00 of the previous day to 05 : 00 of the following one.
- The discharge phase starts at 06 : 20 and finishes at 08 : 30.

Numerical results are related to the $18^{th} January$ 2016, which has been chosen for being the coldest day of that year [14].

The following three-step procedure has been adopted:

1. A first simulation has been run, considering the off-design supply temperature and the design mass-flow rates.
2. The results - in particular the values of T_1 for every substation - have been employed to compute the augmented mass-flow rates, in off-design conditions.
3. A second simulation has been carried out, introducing the values computed at the previous step.

5.1 Effect of the Position

The first, and perhaps most relevant parameter to be investigated is the position of the TES in the network. In fact, its location is likely to change its supply temperature during the discharge phase – depending on the thermal losses that affect the water along the path – and consequently the value of the return temperature that, as already mentioned, affects the thermal load at the plant level.

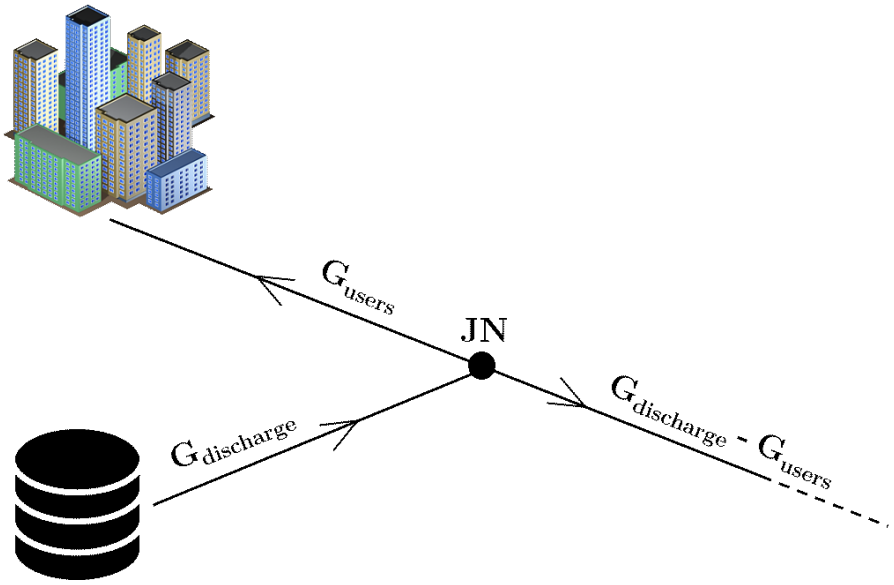

Figure 5.1: Division of the discharged mass-flow rate.

A second aspect is worth considering: with reference to Fig. 5.1, it may be observed that if the size of the tank is big enough, it will be able to inject into the network not only the mass-flow rate G_{users}, required to satisfy the energy demand of all the end-users positioned downstream of the junction node JN, but there will be also a second stream of water leaving JN in the opposite direction. Remembering

Eq. 3.4, the amount of water flowing backwards is bounded by the cross-section of the branch. Therefore, for a storage with pre-selected size, if the diameter of the latter were particularly small (for instance if the tank were linked to a branch directly connected to a a substation), its actual size may shrink to comply with such geometrical limit.
This assumption has been proven observing what happens, after positioning one storage in a more or less favorable position.

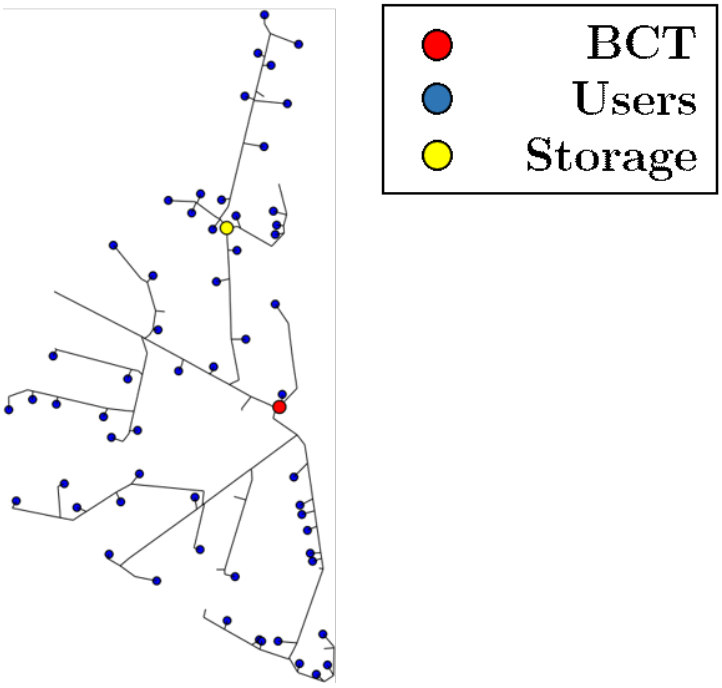

Figure 5.2: Storage located in a favorable position.

In this first case, depicted in Figure 5.2, the branch immediately upstream the junction node has a diameter of $D_{branch} = 150\ mm$. Thanks to its relatively big cross section, it is possible to increase the size of the storage even up to 150 m^3, without breaking any of the boundary conditions of the network.
In order to provide a first glance upon what the consequences of the introduction of a reservoir are, the plots of both the thermal and the pumping load at the *barycentric* node are displayed, and compared to the original ones.
In the figure on the left it may be noticed how the introduction of the storage enabled the plant to endure a far lower pumping load, if compared to design conditions, even though the peak value increased because of the reduced supply temperature when the reservoir is not added (the thinner line in dark red). In the lower left corner of the same plot the small increment in mass-flow rate occurring during the charging phase is observable.

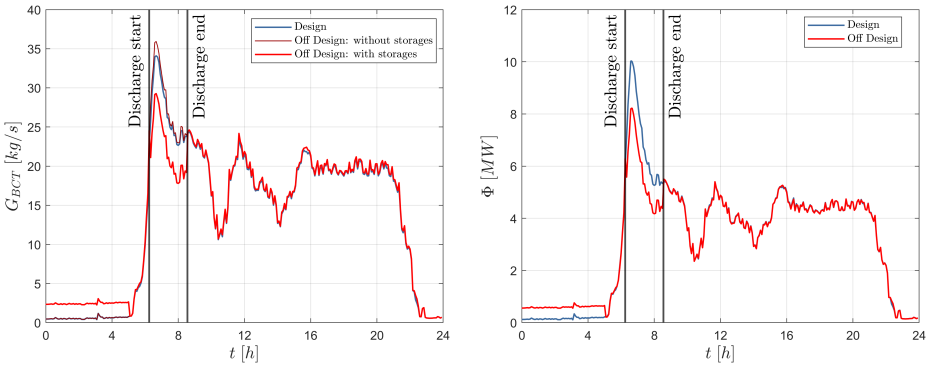

(a) Mass-Flow rate. **(b)** Thermal load.

Figure 5.3: Plots of power and mass-flow rate – $V_{stor} = 50\,m^3$, $T_{BCT} = 114\,^oC$.

A similar behavior relates to the thermal load, displayed in 5.3b: it is worth mentioning how the peak power decreased from more than $10\,MW$ to slightly more than $8\,MW$m thanks to the action of the tank. After the end of the discharge phase instead, the design and off-design curves do match together, in accordance to what has been discussed in Sec. 4.1.1.

One further thing worth highlighting and observing is the representation of the stored and the discharged energy on the plot of the thermal power. In fact, since that the first may be also expressed as the integral over time of the second:

$$E = \int_{t_{start}}^{t_{end}} P(t)\,dt$$

it immediately follows that E corresponds to the area below the curve of the power. More importantly, it should be pointed out that the two surfaces included between the blue and the red curves - during the charging and discharging intervals - are exactly the same, and equal to the MJ of energy stored into all the tanks. Actually, also this statement holds only if buoyancy effects and thermal stratification losses are neglected, as already mentioned in Sec.3.2.2.

Coming back to the optimal positioning of the storage, a second test has been carried out trying to insert a $25\,m^3$ storage in proximity to a substation:
This time the branch connected to the junction node where the tank was in turn linked had a diameter of $D_{branch} = 40\,mm$. Due to its far smaller size, the capacity of the storage was forced to shrink from to $25\,m^3$ to about $15\,m^3$, being the cross-section of the pipe too small, to bear the mass-flow that would have flown through it. From a more realistic point of view, it is as if an existing $25\,m^3$ reservoir

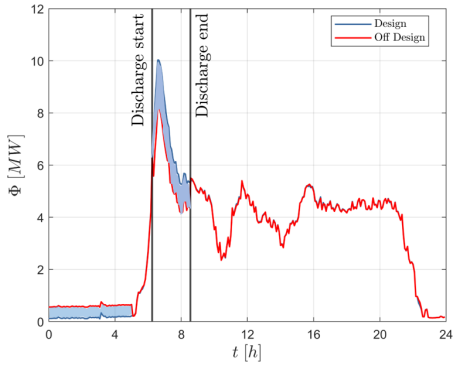

Figure 5.4: Graphical representation of the energy.

had actually been installed, however being able to fill it only up to about 60% of its exploitable capacity. Worthless to say, this is going to have a less satisfactory outcome, in terms of peak reduction.

The same effect, even though due to a different reason, would be obtained if the reservoir would be located close to where the central plant is. Even if there should not be any issues related to the diameters of the pipes, tanks positioned in points like the one depicted in Figure 5.5b would negatively influence the effectiveness of the reservoir itself. In fact, as soon as the discharge starts, the hot water pumped by the facility would soon (actually immediately) mix with the cooler stream leaving the storage – and it could never be otherwise, because the stored water is subject to both insulation and stratification losses – hence reducing its temperature at the very beginning of its path.

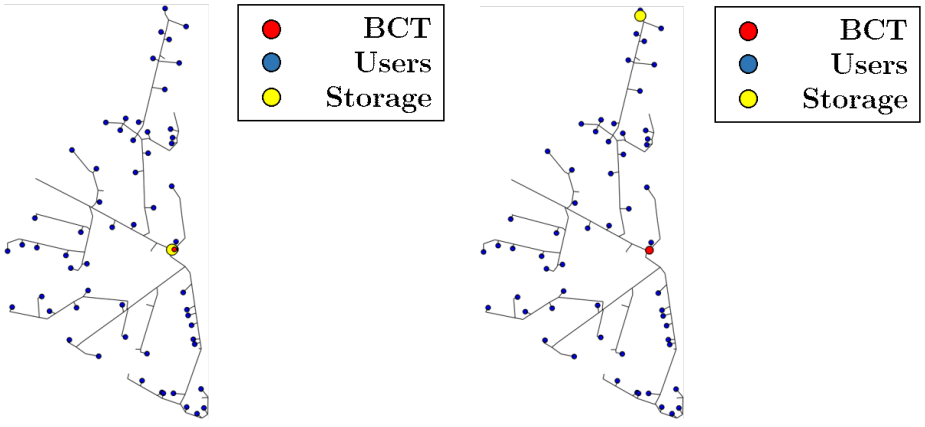

(a) Storage close to a SST. **(b)** Storage close to the plant.

Figure 5.5: Examples of two non favorable positions.

5.2 Best Position: One Storage

Giving the modest dimensions of the network studied in this work, the effect of the introduction of one storage has been evaluated in all the nodes available, for the three sizes already mentioned in the previous section, i.e. $25\,m^3$, $50\,m^3$ and $75\,m^3$. For any of the three cases, the best position was the same and is illustrated on the left in Figure 5.6.
The graphical representation confirms all the inferences made in Sec. 5.1. In fact, the storage is positioned downstream a branch with a diameter of $150\,mm$. Additionally, it is surrounded by a large number of users, with these ones being relatively close to the reservoir itself.

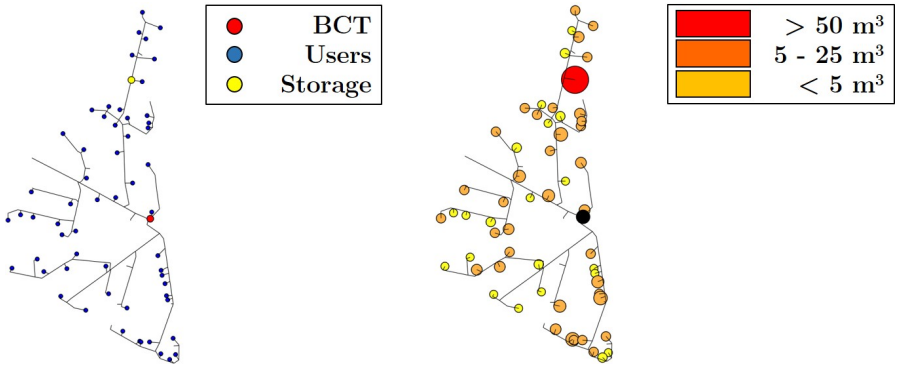

Figure 5.6: Best Position for one TES and volumetric demand of the users.

The figure on the right provides a further, and perhaps the main reason, about why such position is the optimal one. The end-users have been coloured according to the size a storage should have, in order to satisfy their demand during the course of the discharge period, and the radii of the circles are proportionate to their effective requirements. At first glance, it is noticeable that there is one user, whose volumetry is by far the highest among all the buildings attached to the DH network, and it is basically located next to where the reservoir is.
This is the definitive and doubt-clearing confirmation of why the best position could not be anywhere but here. In fact, apart from setting no constraints to the size of the storage, the latter is located by what is basically the largest sinkhole of energy of the whole network, thus optimizing the ratio between the delivered amount of water and the distance it has to travel, i.e. the thermal losses it would be subject to along the path.

The following figures illustrate the effect of the size of the storage on both the pumping and thermal load of the plant.
As one might have expected, the larger the capacity of the storage is, the more

pronounced the peak reduction will be. Numerical results reveal that with the smallest storage available – the $25\,m^3$ one – the peak value of power decreased from about $10\,MW$ to a little more than $9\,MW$, while the $50\,m^3$ and $75\,m^3$ ones enabled to push the top value down to about $8\,MW$ and $7\,MW$, respectively.

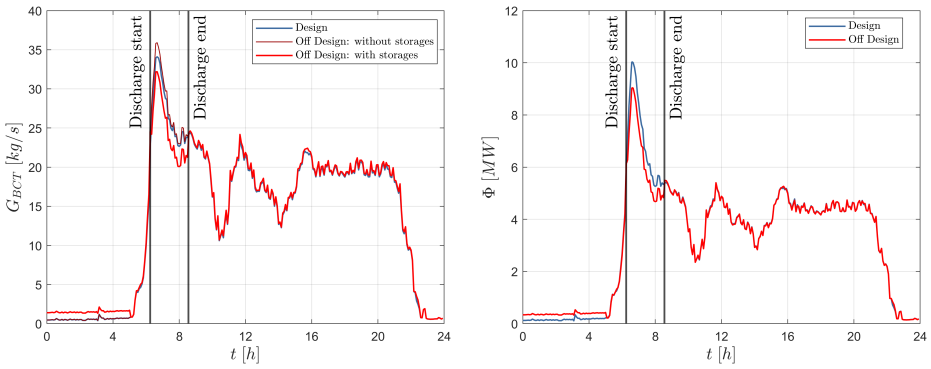

(a) Mass-Flow Rate **(b)** Thermal Load

Figure 5.7: $V_{stor} = 25\,m^3$, $T_{BCT} = 114\,^oC$.

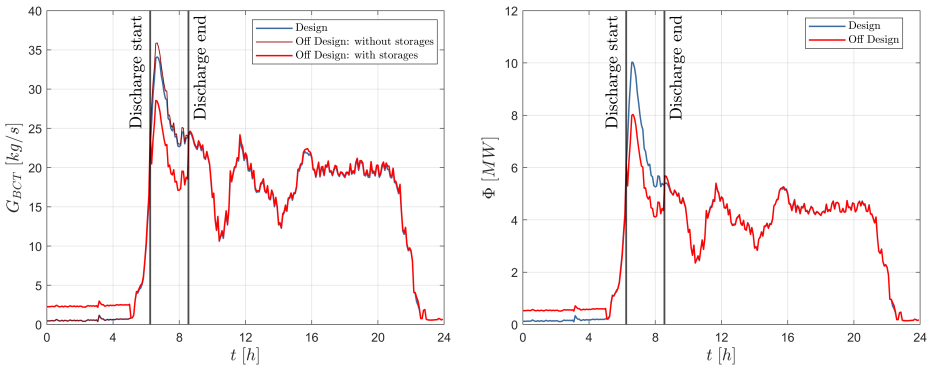

(a) Mass-Flow Rate **(b)** Thermal Load

Figure 5.8: $V_{stor} = 50\,m^3$, $T_{BCT} = 114\,^oC$.

Figure 5.10 illustrates the effectiveness – in terms of peak smoothing effect – of the different positions in which the storage has been tested. The chromatic gradient is proportionate to the relative difference between the maximum value of the thermal load in design conditions and the one evaluated at $T_{BCT} = 114\,^oC$. namely:

$$\Delta P_{\%} = \frac{P_{BCT,max|_{@\,118\,^oC}} - P_{BCT,max|_{@\,114\,^oC}}}{P_{BCT,max|_{@\,118\,^oC}}} \tag{5.2}$$

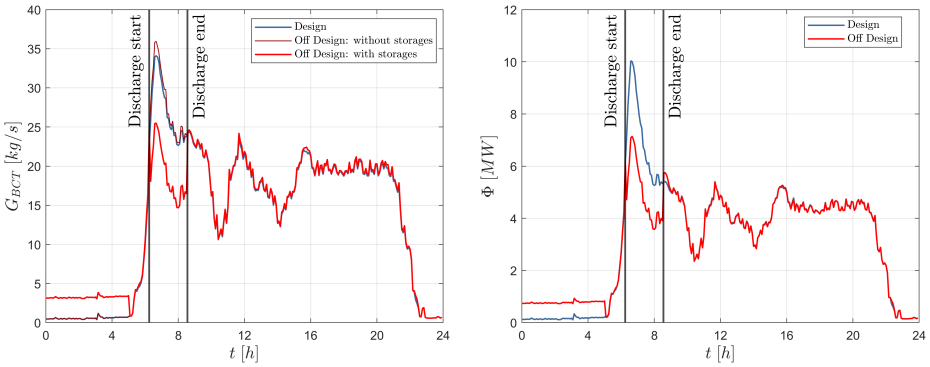

(a) Mass-Flow Rate **(b)** Thermal Load

Figure 5.9: $V_{stor} = 75\,m^3$, $T_{BCT} = 114\,^oC$.

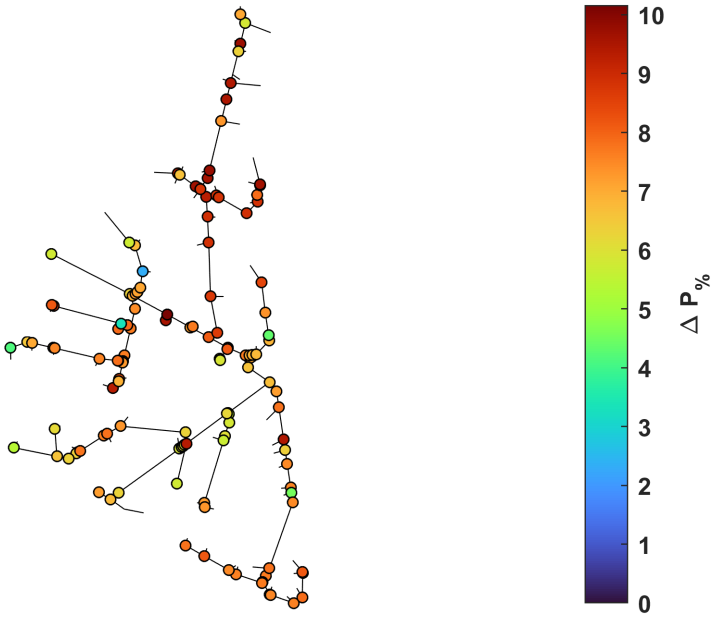

Figure 5.10: Effectiveness of the different positions of the storage - $V_{stor} = 25\,m^3$.

This representation of the network gives an immediate, but even so significant overview of which could be the nodes where the storage would perform better. This may turn out to be useful, particularly if the introduction of more storages were to be accounted for.
It is worth underlining that the figure relates to a $25\,m^3$ and a $T_{BCT} = 114\,^oC$. Since that increasing the size of the reservoir has the consequence of almost rigidly shifting down the off-design curves with respect to the design ones, as illustrated in Fig. 5.8 and 5.9, their relative plots have not been displayed here, since that the

effect of the storage in the different positions would substantially be the same. A different value of the supply temperature would basically not change this configuration as well, but this is going to be explained more in detail in the following section.

The behavior of the return temperature of water at the central plant is worth observing as well.

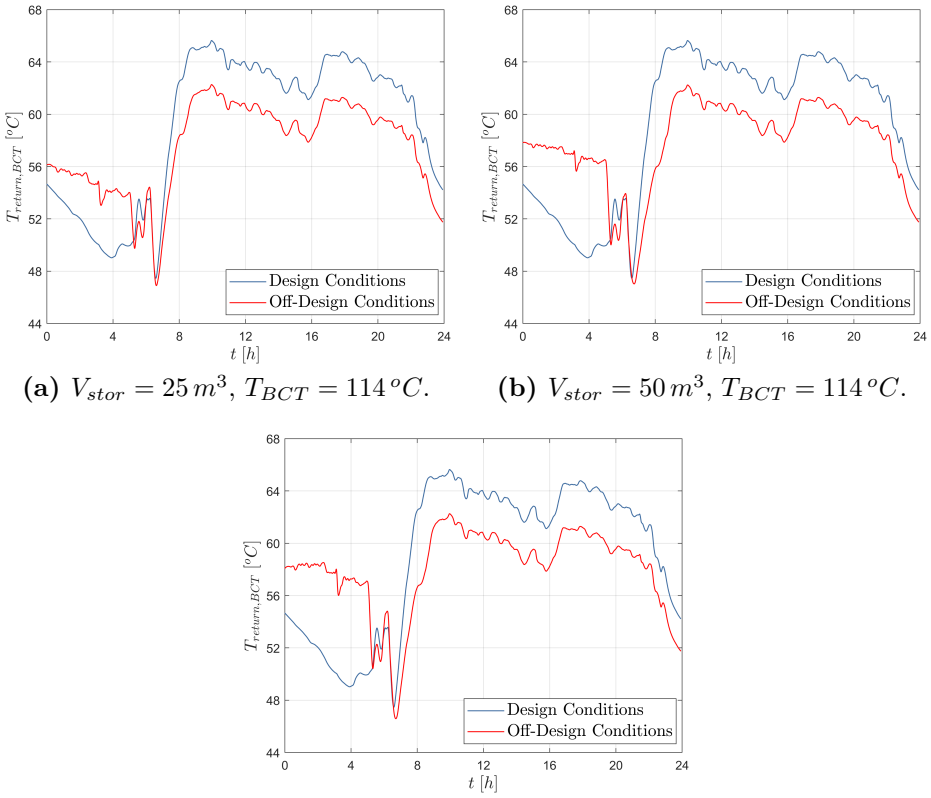

(a) $V_{stor} = 25\,m^3$, $T_{BCT} = 114\,^oC$. **(b)** $V_{stor} = 50\,m^3$, $T_{BCT} = 114\,^oC$.

(c) $V_{stor} = 75\,m^3$, $T_{BCT} = 114\,^oC$.

Figure 5.11: Comparison of Return Temperatures with and without the storage.

The plots do illustrate well how the behavior of the network gets altered during the charging phase. In fact, the larger the storage capacity, the higher, on average, the value of T_{ret} is.

5.3 Effect of the Supply Temperature

A second set of simulations has been carried out choosing a supply temperature of $T_{sup} = 116\,^oC$, to assess what its effect on peak shaving are. Recalling the

expression of the thermal load endured by the central plant:

$$P_{BCT} = G_{BCT}\, c_p \cdot (T_{sup} - T_{ret})$$

it may be observed that a higher supply temperature is likely to make the load increase. Conversely though, the increment in mass-flow rate is going to be lower than the case with a $T_{sup} = 114\,^oC$ displayed in the previous section, hence the final result will be the combination of these two, inverse tendencies.
Numerical results are displayed in the following table, since that they are too close to be distinguished on a plot.

Table 5.1: Peak values for two different supply temperatures.

$\boldsymbol{V_{stor} = 25\,[m^3]}$		
$\boldsymbol{T_{sup}[^oC]}$	$\boldsymbol{P_{max}\,[MW]}$	$\boldsymbol{G_{max}\left[\frac{kg}{s}\right]}$
118	10.03	34.10
116	9.01	31.75
114	9.04	32.19

$\boldsymbol{V_{stor} = 50\,[m^3]}$		
$\boldsymbol{T_{sup}[^oC]}$	$\boldsymbol{P_{max}\,[MW]}$	$\boldsymbol{G_{max}\left[\frac{kg}{s}\right]}$
118	10.03	34.10
116	8.00	28.07
114	8.03	28.55

$\boldsymbol{V_{stor} = 75\,[m^3]}$		
$\boldsymbol{T_{sup}[^oC]}$	$\boldsymbol{P_{max}\,[MW]}$	$\boldsymbol{G_{max}\left[\frac{kg}{s}\right]}$
118	10.03	34.10
116	7.08	25.02
114	7.13	25.48

According to the tables, the case of $T_{sup} = 116\,^oC$ proved to be more advantageous, in terms of peak reduction. Hence, it might be inferred that in spite of the higher value of T_{sup}, the due increase of mass-flow rate was so little, that it yielded a

slightly better improvement, with respect to the tests that had been conducted with a $T_{sup} = 114\,^oC$

The best position of the storage did not change instead. This should not be at any rate surprising, given that the optimal positioning depends on the geometrical properties of the network and on the volumetry of the users surrounding the reservoir itself, but not on the temperature at which water is supplied from the central plant.

Chapter 6

Conclusions

In this work a preliminary, but even so meaningful overview concerning how to lower the supply temperature of an already existing District Heating Network through optimal positioning and sizing of one Thermal Energy Storage has been provided.

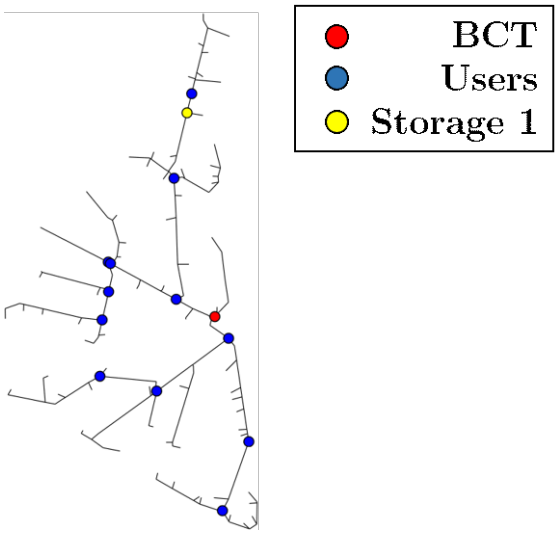

Figure 6.1: Positions tested for two Storages.

The conclusions drawn in the previous chapter can be regarded as reliable and unambiguous, since that the optimal position of the reservoir has been detected among all the possible possibilities. A detailed study involving more than one storage, performed in the same way, would be significantly time consuming, as the number of all the possible combinations would impressively surge up, even with a number of tanks equal to 2.

Nonetheless, a systematically-driven number of tests has been carried out trying to add one more storage in the network starting from the results obtained for the $N_{TES} = 1$ case. Basically, the behavior of the objective function

$$f_{obj} = max(P_{BCT}(t))$$

has been monitored after having positioned the second storage in the most effective positions among the ones displayed in Fig. 5.10, keeping the first in its best position. The chosen points are highlighted in blue in Figure 6.2.
Putting on one side the trivial case of two storages with a capacity of 25 m^3, corresponding to the analysis performed with only one 50 m^3 tank, it may be worth looking at the changes that occurred upon introducing two 50 m^3 reservoirs.

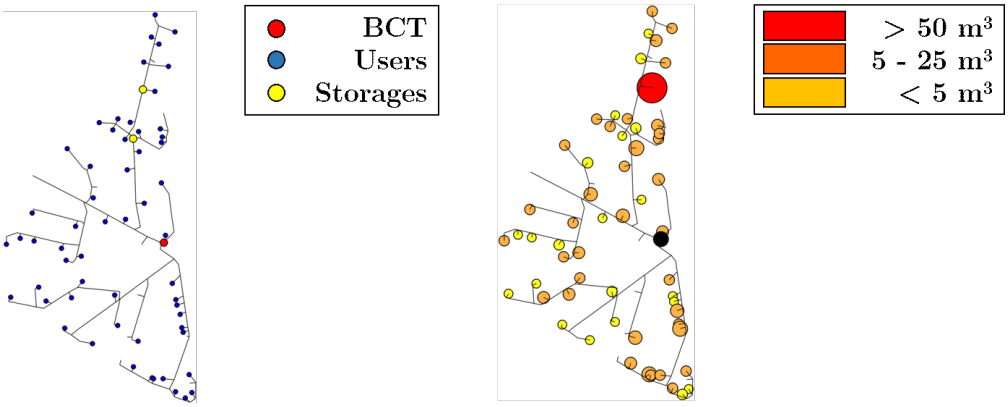

Figure 6.2: Best (presumed) combination of two storages - $V_{stor} = 50\ m^3$.

Observing the position of the second reservoir, together with the map of the volumetric demand of end-users, it may be safely assumed that this two-storages, optimal combination is in accordance with the results shown prior. In fact, the second tank lies along the same, 150 mm diameter branch on which the first had already been positioned. Not only, it must be noted that it is surrounded by numerous end-users, thus underlining the fact that if the whole demand the storage must satisfy is circumscribed in a relatively small area, that spot is likely to be more effective than others.

In spite of the consistency of these tests, if one wished to achieve a more rigorous and reliable result, a finer procedure - for instance an optimization algorithm - should be implemented.
Due to the complexity of the problem, with a large number of factors that may play a fundamental role, an heuristic algorithm may be the right path to follow.

References

[1] Verda V. and Sciacovelli F. «Primary energy savings through thermal storage in district heating networks». In: *Energy (Oxford)* 36 (2011), pp. 4278–4286 (cit. on pp. 1, 18).

[2] Woods P. and Overgaard J. «Historical development of district heating and characteristics of a modern district heating system». In: *Advanced District Heating and Cooling (DHC) Systems*. Woodhead Publishing, 2016. Chap. 1, pp. 3–15 (cit. on p. 1).

[3] Lund H., Werner S., Wiltshire R., Svendsen S., Thorsen J.E., Hvelplund F., and Mathiesen B.V. «4th Generation District Heating (4GDH): Integrating smart thermal grids into future energy systems». In: *Energy (Oxford)* 68 (Apr. 2014), pp. 1–11 (cit. on pp. 1, 2).

[4] Gustafsson J. and Sandin F. «District heating monitoring and control systems». In: *Advanced District Heating and Cooling (DHC) Systems*. Woodhead Publishing, 2016. Chap. 12, pp. 241–258 (cit. on pp. 2, 22).

[5] Cosentino S., Guelpa E., Melli R., Sciacovelli A., Sciubba E., Toro C., and Verda V. «Identification of the optimal operational strategy of a large district heating network through POD modeling». In: *ECOS 2014 - The 27th International Conference on Efficiency Cost, Optimization, Simulation and Environmental Impact of Energy Systems*. Turku, Finland, June 2014 (cit. on p. 2).

[6] Brand M. and Svendsen S. «Renewable-based low-temperature district heating for existing buildings in various stages of refurbishment». In: *Energy (Oxford)* 62 (Oct. 2013), pp. 311–319 (cit. on p. 3).

[7] Wahlroos M., Prässinen M., Manner J., and Syri S. «Utilizing data center waste heat in district heating – Impacts on energy efficiency and prospects for low-temperature district heating networks». In: *Energy (Oxford)* 140 (Dec. 2017), pp. 1228–1238 (cit. on p. 3).

[8] Morandin M., Hackl R., and Harvey S. «Economic feasibility of district heating delivery from industrial excess heat: A case study of a Swedish petrochemical cluster». In: *Energy (Oxford)* 65 (Feb. 2014), pp. 209–220 (cit. on p. 3).

[9] Sciacovelli A., Verda V., and Borchiellini R. *Numerical Design of Thermal Systems*. Turin, Italy: CLUT, 2013 (cit. on p. 6).

[10] Guelpa E. and Verda V. «Thermal Energy Storage in District Heating and Cooling systems: a review». In: *Applied Energy* 252 (Oct. 2019), p. 113474 (cit. on p. 13).

[11] Colella F., Sciacovelli A., and Verda V. «Numerical analysis of a medium scale latent energy storage unit for district heating systems». In: *Energy (Oxford)* 45 (May 2012), pp. 397–406 (cit. on p. 13).

[12] *Introduction to Thermal Systems Engineering: Thermodynamics, Fluid Mechanics, and Heat Transfer*. New York, USA: John Wiley & Sons, Inc., 2003 (cit. on p. 23).

[13] *Techno System: descrizione e teoria*. Tech. rep. Certaldo, Italy: Techno System, 2020 (cit. on p. 25).

[14] *Il clima in Piemonte nel 2016*. Tech. rep. Turin, Italy: ARPA Piemonte, 2017 (cit. on p. 28).